

Electronic Supplementary Information

Biomolecules-guided co-localization of intermolecular G-rich strands for construction of tetramolecular G-quadruplex sensing strategy

Changjia Hu ^{a,b}, Yanwen Jin ^a, Peng Yang ^b, Rongxing Zhou ^a, Lingying Xia ^{a,b}, Lijie
Du ^b, Junbo Chen ^{*b}, Nansheng Cheng ^{*a}, Xiandeng Hou ^b

^a Biliary Surgical Department, West China Hospital, Sichuan University, Chengdu,
Sichuan, China, 610225

^b Analytical & Testing Center, Sichuan University, 29 Wangjiang Road, Chengdu,
610064, China.

E-mail: junbochen@scu.edu.cn and nanshengcheng@hotmail.com

1. Reagents and Materials

DNA sequences (Table S1) in this work were synthesized and purified by Sangon Biotech. Co., Ltd. (Shanghai, China). DNA powders were dissolved and diluted by ultrapure water ($\geq 18.2 \text{ M}\Omega \text{ cm}^{-1}$) and stored at -20°C .

H_2O_2 , citric acid (CA), acetic acid (HAc), KCl, MgCl_2 , HCl, NiCl_2 , NaOH and dimethyl sulfoxide (DMSO) were from Chron Chemicals Co., Ltd (Chengdu, China). $(\text{NH}_4)_2\text{HPO}_4$ and hemin were brought from Aladin (Shanghai, China). D-biotin, and native PAGE preparation kit were purchased from BBI Solution (Shanghai, China). 2,2' Azino-bis(3-ethylbenzothiazoline-6-sulfonic acid) (ABTS) and Thioflavin T (ThT) were ordered from Diamond (Shanghai, China) and Shanghai Yuanye Biotechnology Co., Ltd (Shanghai, China), respectively. Recombinant human platelet-derived growth factor-BB (PDGF-BB), D-Biotin, 5×TBE buffer, TE-Mg buffer, Tris-HCl buffer, HEPES buffer and 10×PBS buffer were commercially obtained from Sangon Biotech. Co., Ltd. (Shanghai, China). 6 × Loading buffer and marker A used in electrophoresis were purchased from Takara Biomedical Technology Co., Ltd. (Dalian, China). Streptavidin (SA) was obtained from New England Biolabs Ltd. (Beijing, China). Hemoglobin (HEMO) was purchased from Sigma-Aldrich (Shanghai, China). Mucin was ordered from Diamond (Shanghai, China). Immunoglobulin G (IgG), transferrin (TRF), and human serum albumin protein (HSA) were purchased from Bioss Biotech. Co., Ltd. (Beijing, China).

Estimation of the melting temperature (T_m) and delta G of hybrid was calculated by IDT Oligo Analyzer and evaluation of the reaction between oligonucleotides was

also simulated by NUPACK. Except that hemin was dissolved in DMSO, the rest reagents were dissolved or diluted by ultrapure water and stored at 4°C without special mention. All the reagents were at least analytical grade.

Table S1. Sequences of All DNA Oligonucleotides Used in This Work

Name	Sequence (5'- 3')
G-rich Strand-2	TTT TTT TTT TTT TTT TTT TT AAA AGG
G-rich Strand-4	TTT TTT TTT TTT TTT TTT TT AAG GGG
G-rich Strand-6	TTT TTT TTT TTT TTT TTT TT GGG GGG
G-rich Strand-8	TTT TTT TTT TTT TTT TTT TT GGG GGG GG
G-rich Strand-10	TTT TTT TTT TTT TTT TTT TT GGG GGG GGG G
Guider	AAA AAA
SA-G Strand	Biotin-TTT TTT TTT TTT TTT TTT TT GGG GGG
HCV DNA	TAG CGT TGG GTT GCG AAA GGC CTT GT
Blocker for HCV	GCC TTT CGC AAC CCA ACG CTA TTT TT AAA AAT AGC GTT GGG TTG AAA AAA AAA AAA AAT AGC GTT GGG TTG AAA AAA AAA AAA AAT AGC GTT GGG TTG AAA AAA AAA AAA AAT AGC GTT GGG TTG
Guider for HCV	AAA AAT AGC GTT GGG TTG AAA AAA AAA AAA AAT AGC GTT GGG TTG AAA AAA AAA AAA AAT AGC GTT GGG TTG AAA AAA AAA AAA AAT AGC GTT GGG TTG
G Strand 1 for HCV	AAC GCT ATT TTT AAA AAA AAA AGG GGG G
G Strand 2 for HCV	CAA CGC TAT TTT TAA AAA AAA AAG GGG GG
G Strand 3 for HCV	CAA CGC TAT TTT TAA TAA TAA TAG GGG GG
G Strand 4 for HCV	CCA ACG CTA TTT TTA AAA AAA AAA GGG GGG
G Strand 5 for HCV	CCA ACG CTA TTT TTA ATA ATA ATA GGG GGG
HAV DNA	TTA GAG TTG CAT GGA TTA ACT CCT CTT TCT
HBV DNA	CAA CCT CCA ATC ACT CAC CAA CCT CCT

Random 1	AAG CGT GTA TCC CAT GTG TCC GTG TGA TG
Random 2	TTT TTT TTT TTT AGT CCG TGG TAG GGC
Guider with PDGF-BB aptamer	<u>AAA AAA ACA GGC TAC GGC ACG TAG AGC</u> <u>ATC ACC ATG ATC CTG AAA AAA AAA AAA</u> <u>AAA CAG GCT ACG GCA CGT AGA GCA TCA</u> <u>CCA TGA TCC TGA AAA AAA</u>
G Strand 1 for PDGF-BB	<u>GTA GCC TGT TTT TTA</u> ATA ATA ATA GGG GGG
G Strand 2 for PDGF-BB	<u>TTT TTT CAG GAT CAT AAT AAT AAT</u> AGG GGG G

2. Apparatus

The CD data were collected from 230 nm to 330 nm at room temperature with Chirascan Plus qCD (Applied Photophysics Ltd., UK). The gel was stained by GelRed and then imaged with ChampGel 7000 (China). All the spectral absorption and fluorescence measurements in this experiment were completed by BioTek H1M (USA). AFM imaging was performed using Cypher VRS (Oxford Instrument, UK). Ultrapure water was prepared by a purification system from PINCHENG (Pure Technology CO., Ltd., China).

3. PAGE Analysis

To prepare a 12% polyacrylamide gel about 10 mL, the native PAGE preparation kit is helpful. 2 mL of 5×TBE and 4 mL of 30% Acr-Bis (29:1) was added into 4 mL ultrapure water, and then 100 μ L of 10% ammonium persulfate (APS) and 6 μ L of N,N,N',N'-tetramethylethylenediamine (TEMED) were rapidly mixed with the solution and stood still to trigger polymerization for 1 h at room temperature.

G-rich Strand and **Guider** were diluted to a final concentration of 1 μ M and 0.25 μ M, respectively. The volume of each sample was 10 μ L and was proportionally mixed with 2 μ L of 6×loading buffer. Then, each sample was loaded into the notches of the 12% PAGE.

Electrophoresis was conducted at 120 V for about 1 h, and then the gel was stained with GelRed and imaged.

The operation of PAGE preparation is different to the above when the guider is SA. To allow the band of SA-guided G-quadruplex to go down, 8% PAGE was prepared. 3 mL of 5×TBE and 4 mL of 30% Acr-Bis (29:1) was added into 9 mL ultrapure water, and then 180 μ L of 10% ammonium persulfate (APS) and 9 μ L of N,N,N',N'-tetramethylethylenediamine (TEMED) were rapidly mixed with the solution and stood still to trigger polymerization for 1 h at room temperature.

4. Preparation for AFM

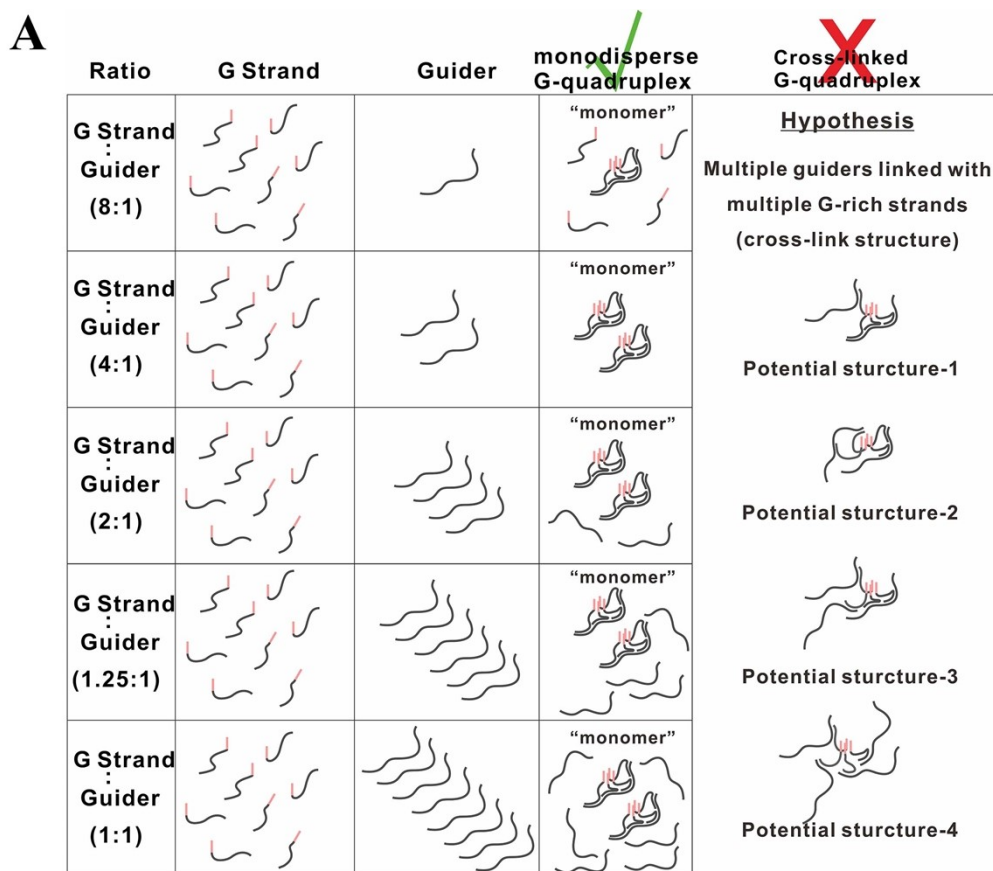
AFM on DNA samples (**G-rich Strand** and **Guider** induced intermolecular G-quadruplex) were performed on the mica surface. Before the loading of DNA sample, the mica was treated with isopropanol and ethanol for ten-minute ultrasonic cleaning, respectively. Then 10 μL of 1 μM DNA sample in buffer (Tris-HCl with 100 mM KCl and 50 mM MgCl_2 , pH 7.4) and 10 μL of 50 mM NiCl_2 in water were deposited on the mica surface, incubated for several minutes and finally rinsed.

The operation is the same when the guider is SA, except the concentration. We use 0.1 μM SA-G Strand and 0.025 μM SA to make it sparser in the AFM imaging.

5. Preparation of G-rich Strand Probe for AFP Detection

After 92 μL TE-Mg buffer was added into a 200 μL -PCR tube A, 4 μL of 5 μM streptavidin (SA) and **SA-G Strand** were added successively. After slight vortex mixing, **SA:SA-G Strand** was obtained by incubation at room temperature for 1 h. Then 85 μL of TE-Mg buffer and 15 μL of 0.2 mg / ml ($\sim 1.3 \mu\text{M}$) anti-AFP antibody were added into another 200 μL -PCR tube B. The solution in tube A and B was mixed evenly, and then incubated at room temperature for 1 h to get the probe **AFP:SA:SA-G Strand**, which denoted as AFP-G. Finally, 10 μL of 1 mM biotin was added into the solution and incubated overnight in the refrigerator at 4 $^{\circ}\text{C}$ to block the redundant sites of SA. The prepared probe **AFP-G** (100 nM) was stored at 4 $^{\circ}\text{C}$ for use.

6. To confirm that signals were generated from inner G-quadruplex (monodisperse)



↓ The intensity **did not enhance** as the increased concentration of guider molecules

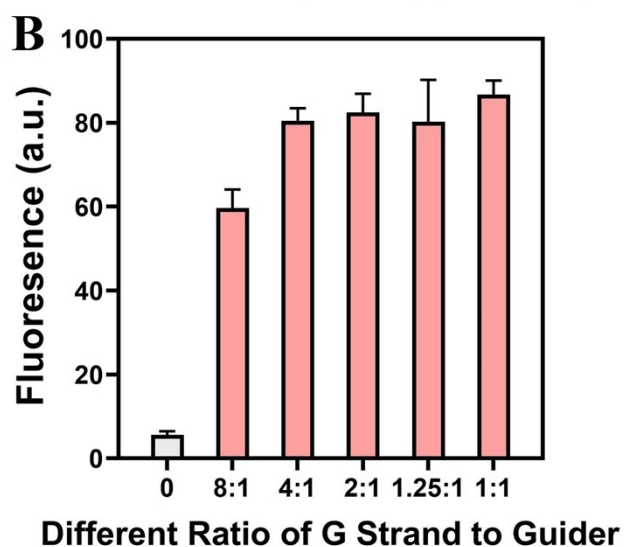


Figure S1. (A) Typical formation of inner G-quadruplex (monodisperse) and hypothesized cross-linked G-quadruplex (Rarely existed in our design). (B) The intensity of groups with different ratio of G-strand to guider, including 8:1, 4:1, 2:1, 1.25:1 and 1:1. we adjust the concentration of guider to increase the chance of cross-linked DNA structure formation. By fixing the concentration of G-

rich strands, the concentration of guider was sequentially increased to establish the several reaction groups with different ratio of G-strand to guider. In each group, ThT was employed as fluorescent substrate to generate the intensity.

Theoretically, the more molecules existed, the more complex structures are prone to be formed, thus, we adjust the concentration of guider to increase the chance of cross-linked DNA structure formation. Under the circumstance (e.g., the reaction group of 1:1) in favor of the formation of the cross-link structure, if the excessive guider molecules were preferred to be assembled with G-rich strands as cross-link structure, those structure would generate the high intensity. In each group, ThT was employed as fluorescent substrate to generate the intensity. As result, the intensity of from 2:1 group to 1:1 group did not enhance as the increased concentration of guider molecules

7. The formation of intermolecular G-Strand was characterized by the circular dichroism (CD) test, native PAGE analysis and Atomic Force Microscopy (AFM)

To further characterize the extent for G-quadruplex formation from G Strand and Guider induced intermolecular G-quadruplex, AFM imaging was obtained and shown in Figure S2. Imaging from Guider induced intermolecular G-quadruplex has more mountain shapes than that from G Strand only, which indicated efficient formation of G-quadruplex.

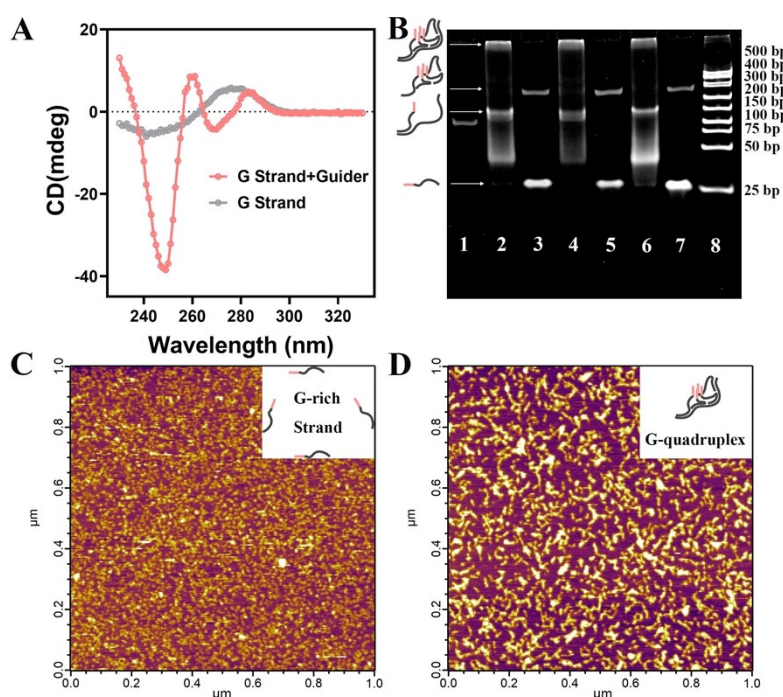


Figure S2. (A) Circular dichroism characterization, with CD data collected from 230 nm to 330 nm at room temperature; (B) electrophoresis characterization: Lane 1:guider only; Lanes 2, 4 and 6: guider + G-Strand; Lanes 3, 5 and 7: G- only, and Lane 8: Mrker A; and (C) and (D) AFM images with the scale bar of 100 nm corresponding to free G-Strand and co-localized G-Strand, respectively..

8. Atomic Force Microscopy (AFM) Imaging and analysis

To further characterize the extent for G-quadruplex formation from G Strand and Guider induced intermolecular G-quadruplex, AFM imaging was obtained and shown in Figure S2. Imaging from Guider induced intermolecular G-quadruplex has more mountain shapes than that from G Strand only, which indicated efficient formation of G-quadruplex.

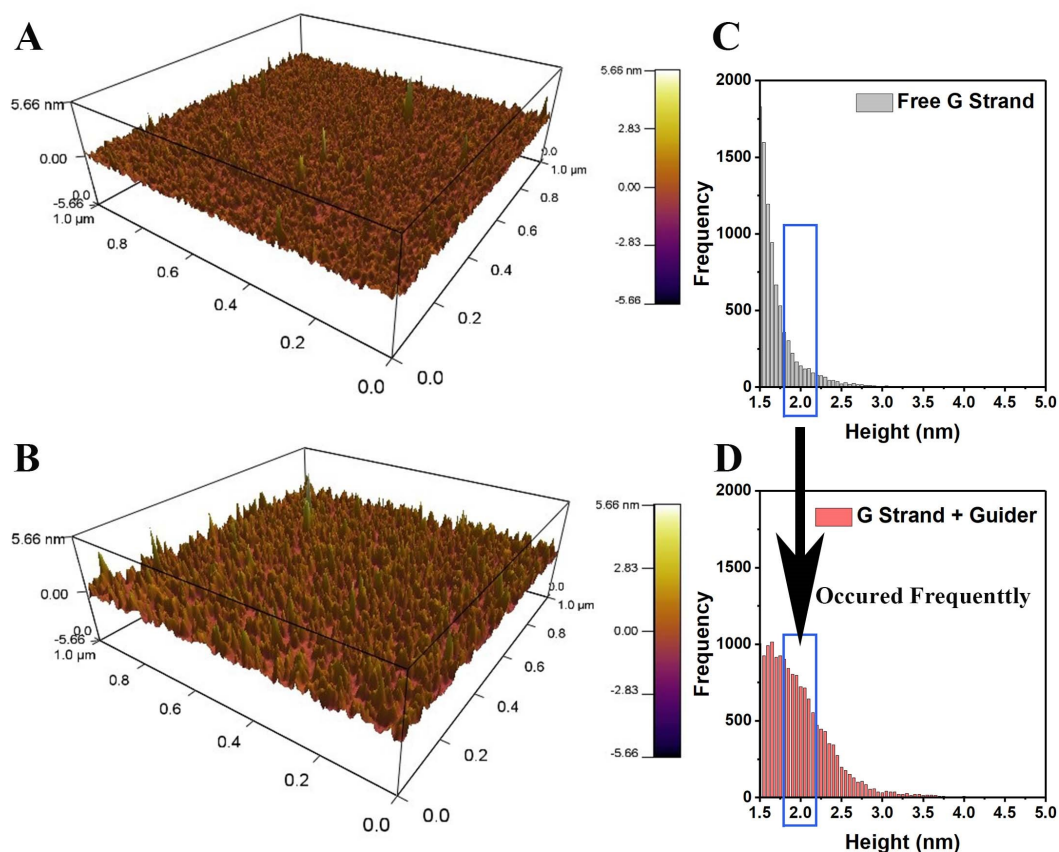


Figure S3. The characterization of free G Strand and the G-quadruplex from co-localized G Strand. AFM 3D imaging for (A) free G Strand and (B) assembled G-quadruplex. The height profiles of (C) free G Strand and (D) G-quadruplex induced by G-rich Strand + Guider. We assigned the Y-axis as the frequency of occurrence of specific DNA structure, the X-axis as the height of specific DNA structure. Particularly, the lower value of Y-axis indicated the less occurrence of its corresponding DNA structure. The higher value of Y-axis indicated the more occurrence. According to the previous studies, the values for G-quadruplex determined by AFM was around 2 nm.⁶⁻¹⁰ By adding the Guider, the specific DNA structures around 2 nm are occurred frequently.

9. Optimization of Guanine Bases Number by ABTS

Since hemin can combine with G quadruplex to greatly enhance its capability of catalysis, ABTS was used as the substrate here, and the formed G quadruplex interacts with hemin to make ABTS oxidized in the presence of hydrogen peroxide, and the color changes from colorless to green.

To optimize the number of guanine bases in **G Strand**, 2 to 10 of guanine bases at the 5'-terminus were chose. Figure S3 shows that **G Strand** with 6 guanine bases owned the best signal with **Guider** and relative low background without **Guider**.

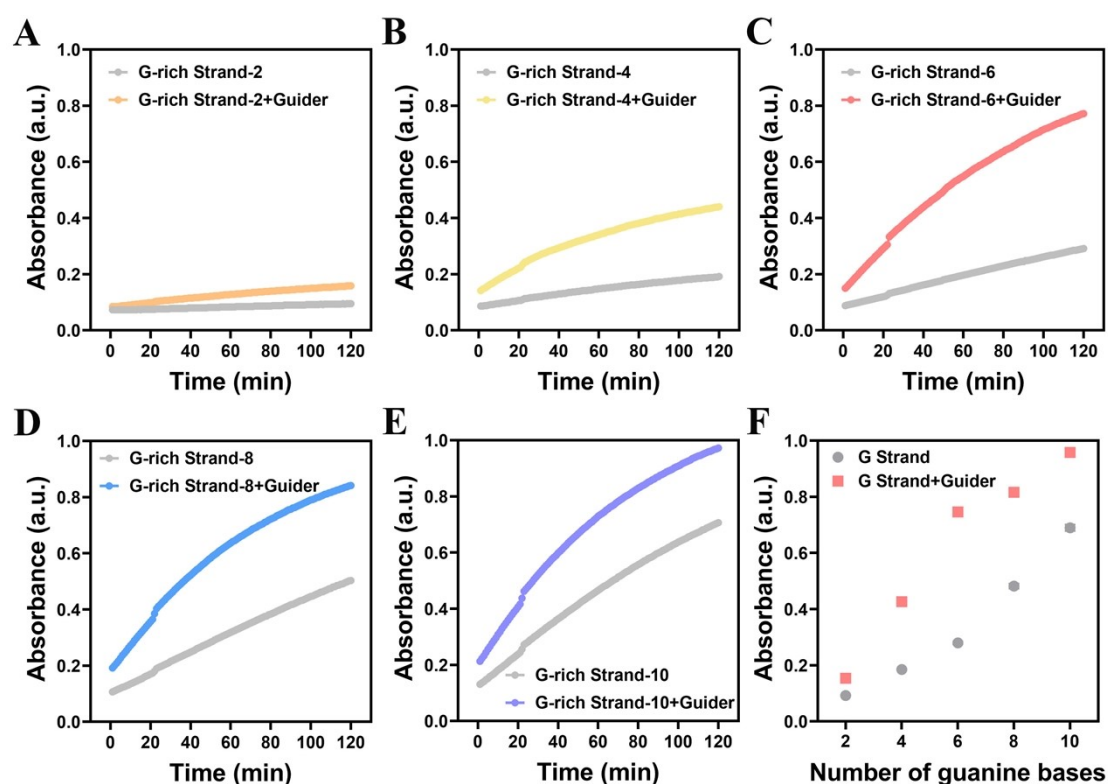


Figure S4. Optimization of guanine base number: (A) 2 guanine bases; (B) 4 guanine bases; (C) 6 guanine bases; (D) 8 guanine bases; (E) 10 guanine bases; and (F) optimization of guanine bases number from 2 to 10 by ABTS. Absorbance measurements were taken at 120 min (420 nm).

10. Optimization of Guanine Bases Number by ThT

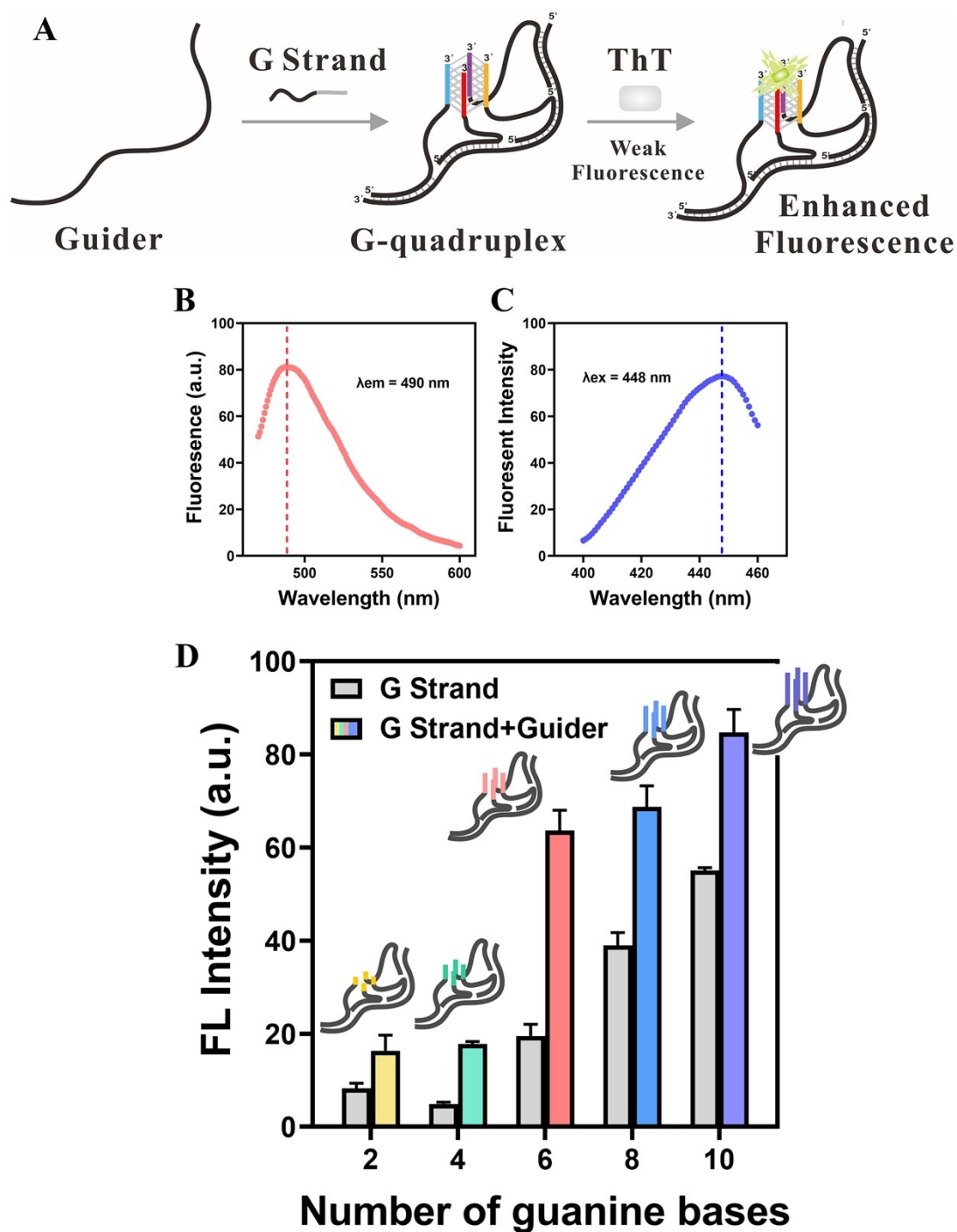


Figure S5. (A) Schematic illustration of guider induced intermolecular G-quadruplexes self-assembly. ThT plays a role of fluorescence signals output; (B) optical emission spectrum; (C) optical excitation spectrum of ThT; and (D) optimization of guanine bases number from 2 to 10 by ThT. Fluorescence measurements were taken immediately.

In fact, the native fluorescence of ThT is very weak in solution. A slight increase

in the fluorescence will appear after the addition of the **G-rich Strand**. The ignorable fluorescent intensity (FI) can be treated as the background and the other one greatly enhanced via the formed intermolecular G-quadruplex induced by **Guider** can be regarded as the target signal.

To detect the signal of ThT, we tested the excitation and emission spectrum of ThT to get the maximum excitation wavelength λ_{ex} (448 nm) and maximum emission wavelength λ_{em} (490 nm) in Figure S4C and Figure S4B. When we optimized the number of guanine bases in **G-rich Strand**, 2 to 10 of guanine bases at the 5'-terminus were chosen and added ThT as the fluorescent signal output. Figure S4D showed consistent results with Figure S3 that **G-rich Strand** with 6 guanine bases owned the best signal with **Guider** and relative low background without **Guider**.

11. Ratio Investigation of G Strand to Guider

G-quadruplex assembly in our strategy was achieved by the co-localization of four intermolecular G Strand. So we tested different ratio of G Strand to the Guider.as shown in Figure S5, a ratio of 4:1 yielded the highest signal, which corresponded to the co-localization of four G Strand.

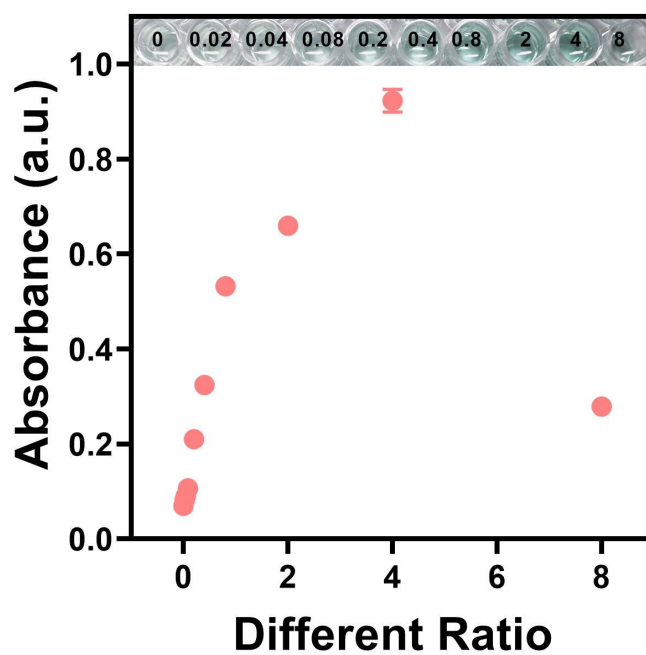


Figure S6. Ratio investigation of G Strand to Guider. Absorbance measurements were taken at 120 min (420 nm).

12. Investigation of G-rich Strand and Guider Concentration on Formation Effect of Tetramolecular G-quadruplex

High concentration of **G-rich Strand** may trigger the formation of G-quadruplex, but too low concentration of G may give an unobvious signal that we cannot realize the function of **Guider**. So, we investigate different concentrations of **G-rich Strand** and **Guider** with a fixed ratio of 4:1 due to the result of Figure S5. As shown in Figure S6, with the increase of **G-rich Strand** and **Guider** concentrations, both signal and background are rising. We chose a moderate concentration of 1 μM of **G-rich Strand** and 0.25 μM of **Guider** with good signal-to-noise ratio as the experimental concentrations.

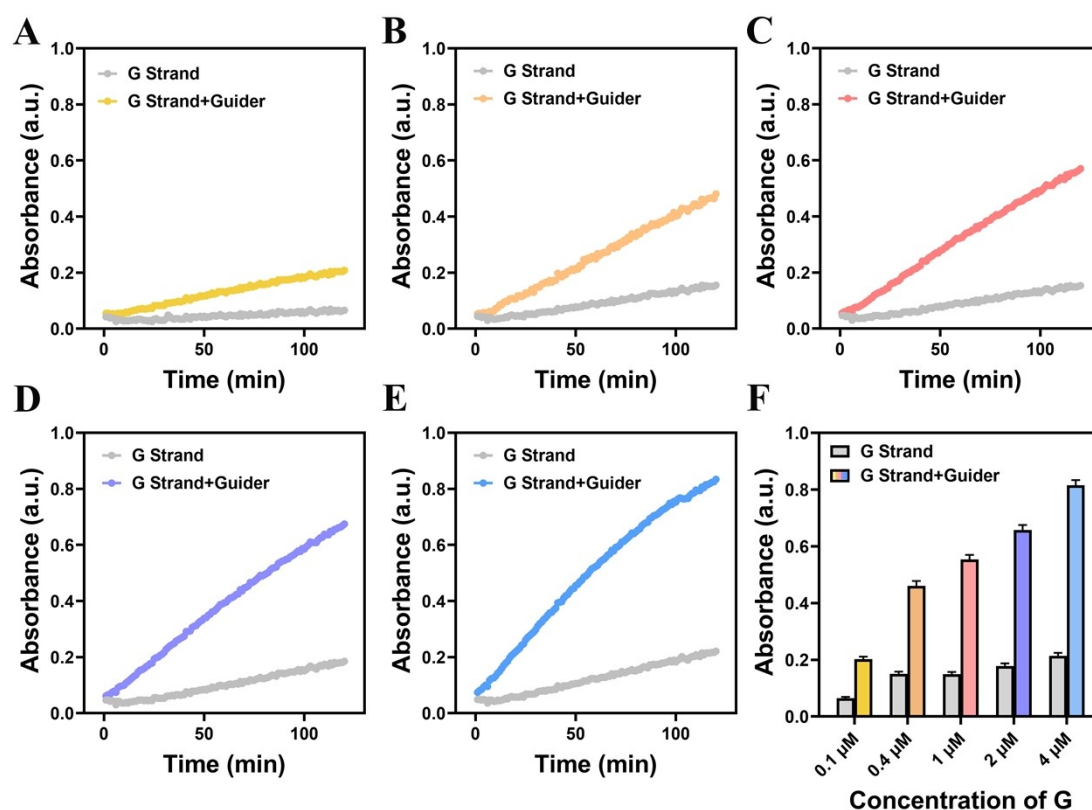


Figure S7. Concentration optimization of **G-rich Strand** and **Guider** with a fixed ratio of 4:1: (A) 0.1 μM **G-rich Strand** and 0.025 μM **Guider**; (B) 0.4 μM **G-rich Strand** and 0.1 μM **Guider**; (C) 1 μM **G-rich Strand** and 0.25 μM **Guider**; (D) 2 μM **G-rich Strand** and 0.5 μM **Guider**; (E) 4 μM **G-rich Strand** and 1 μM **Guider**; and (F) absorbance of different concentration of **G-rich Strand** in this reaction with or without **Guider** of corresponding concentration. Absorbance measurements were taken at 120 min (420 nm).

13. Investigation of Outer Reaction Conditions on Formation Effect of Tetramolecular G-quadruplex

Considering the reaction buffer, cation strength and pH value are crucial for the formation of G-quadruplex with peroxidase-mimicking capability to generate the signal, we then investigated the effect of several outer conditions on the formation of tetramolecular G-quadruplex. Several common buffers were selected: $(\text{NH}_4)_2\text{HPO}_4$ -CA, Tris-HCl, Tris-HAc, HEPES, and PBS, in which 10 mM KCl was added to stabilize the G-quadruplex. $(\text{NH}_4)_2\text{HPO}_4$ -CA has a slightly acidic pH, and according to the literature, NH_4^+ can assist to stabilize the G-quadruplex,^{1, 2} so it has the best performance. Then, by adjusting the ratio of $(\text{NH}_4)_2\text{HPO}_4$ and CA in $(\text{NH}_4)_2\text{HPO}_4$ -CA buffer, the pH of buffer solution is adjusted to 4, 5, 6, 7, 8, respectively. When pH is 5, the highest signal is displayed, because ABTS is easier to color in this relatively acidic condition.^{3, 4, 5} At the same time, it was observed that even the buffer solution with low concentration could have a considerable signal.

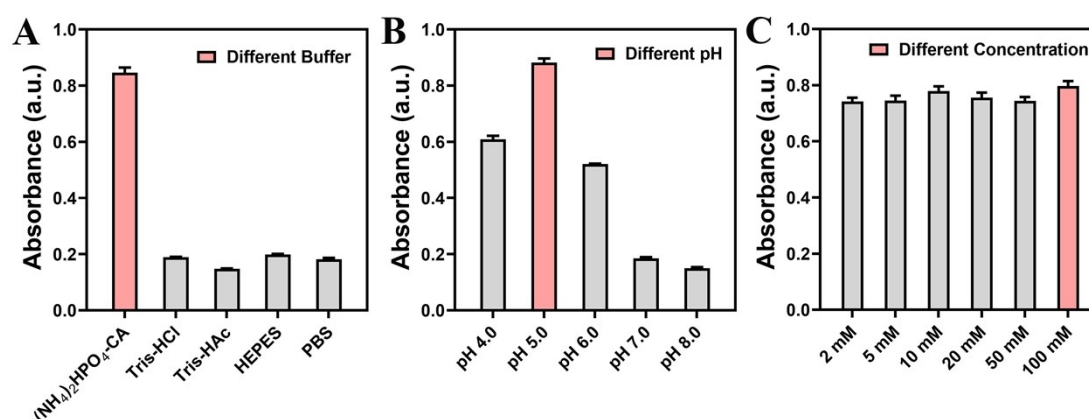


Figure S8. Optimization of buffer type (A), buffer pH (B) and buffer concentration (C). Absorbance measurements were taken at 60 min (420 nm).

14. Investigation of ABTS Concentration on Signal Output

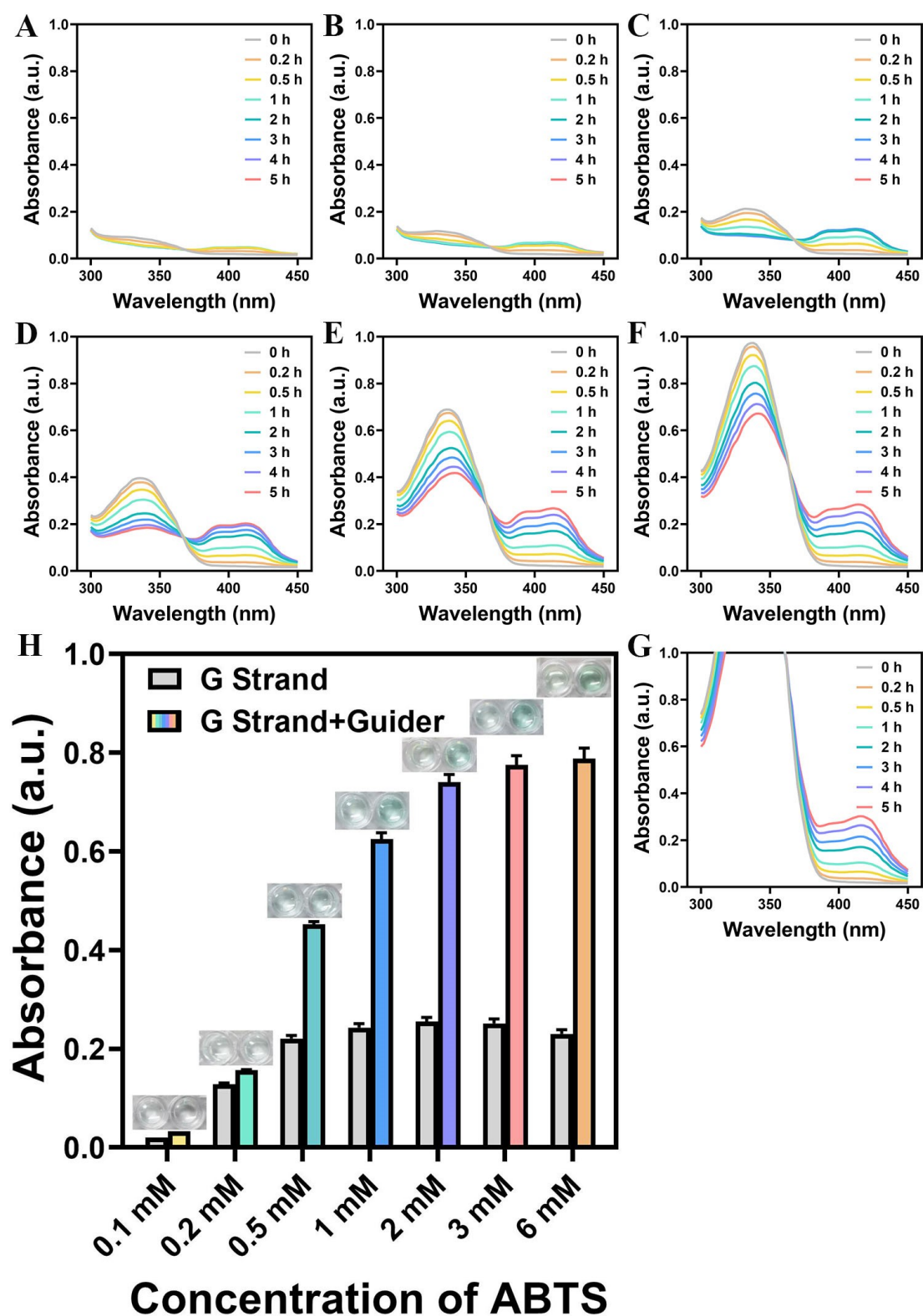


Figure S9. Concentration optimization of ABTS: (A) 0.1 mM, (B) 0.2 mM, (C) 0.5 mM, (D) 1 mM, (E) 2 mM, (F) 3 mM, (G) 6 mM; (H) Absorbance and color comparison in this reaction with or without **Guider** in different concentration of ABTS. Absorbance measurements were taken at 120 min (420 nm).

ABTS was used as the oxidation substrate in the visual experiment, and its concentration will also affect the final experimental results. So, we investigated different concentrations of 0.1 mM, 0.2 mM, 0.5 mM, 1 mM, 2 mM, 3 mM, and 6 mM. However, 0.1 mM and 0.2 mM ABTS were too low to discriminate the color change, and please note the data were not shown here. As can be seen in Figure S8, with the increase of ABTS concentration, the color contrast between the experiment with and without **Guider** is more obvious, but the peak intensity at 340 nm of ABTS with too high concentration (6 mM) is overflow, so 3 mM ABTS is selected as the final experimental concentration.

15. Investigation of H₂O₂ Concentration on Signal Output

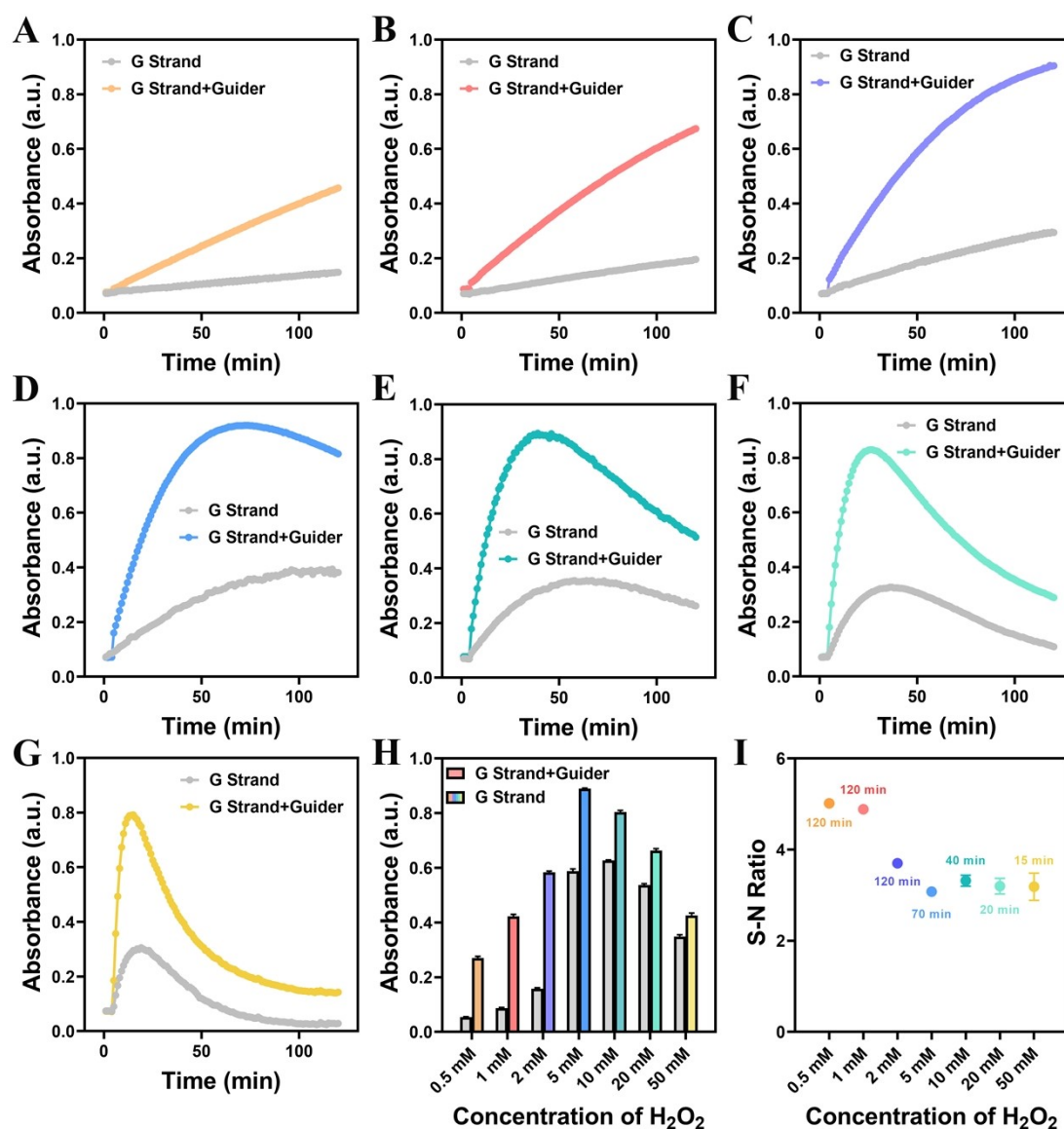


Figure S10. Concentration of H₂O₂: (A) 0.5 mM, (B) 1 mM, (C) 2 mM, (D) 5 mM, (E) 10 mM, (F) 20 mM, (G) 50 mM and (H) absorbance of different concentration of H₂O₂ in this reaction with or without **Guider**. (I) Signal-to-noise ratio for different concentration of H₂O₂. Absorbance measurements were taken at the time of their best signal-to-noise ratio point (420 nm): 120 min, 120 min, 120 min, 70 min, 45 min, 20 min, and 15 min, respectively.

As an oxidant in the visual signal output part of this experiment, the concentration of hydrogen peroxide (H₂O₂) is also essential. So, we used the concentration of 0.5 mM, 1 mM, 2 mM, 5 mM, 10 mM, 20 mM, and 50 mM H₂O₂ for the test. As shown in Figure S9, the reaction speed is accelerated with the increase of H₂O₂ concentration. The maximum absorption of H₂O₂ with 50 mM can be achieved in about 20 min. However,

it can be seen from the comparison of signal-to-noise ratio in Figure S9I, with the increase of hydrogen peroxide concentration, the signal-to-noise ratio will slightly decrease.

Because of no special requirements for the reaction time at present, we chose 1 mM H_2O_2 with moderate time and signal as the experimental concentration. If the subsequent reaction time is required, the H_2O_2 concentration can be increased at the expense of less signal-to-noise ratio.

16. Investigation of Guider Concentration to Co-localization of Intermolecular G Strand for Construction of Tetramolecular G-quadruplex

To demonstrate the formation efficiency of tetramolecular G-quadruplex is proportional to the **Guider**, we hereby investigated the response of this strategy to various concentrations of **Guider** by absorption (Figure S10A) and fluorescence (Figure S10B), exhibiting a guider concentration dependent trend.

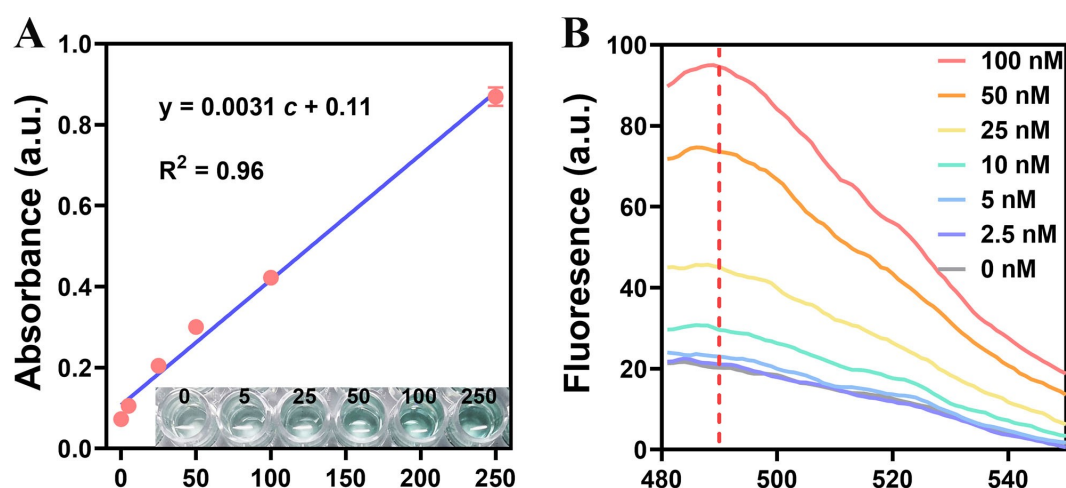


Figure S11. (A) Fluorescent response to various concentration of **Guider** by ThT ($\lambda_{ex} = 448$ nm) and (B) absorbance response to various concentration of Guider by ABTS (420 nm). Absorbance measurements were taken at 120 min (420 nm) and fluorescence measurements were taken immediately.

17. Investigation of Effect of G-Strand with Different Toeholds on HCV DNA Detection

Because the constructed HCV DNA sensing strategy is based on the competitive hybridization of HCV DNA and Guider for HCV to Blocker for HCV, and the competitive hybridization of G Strand to HCV and Blocker to Guider for HCV, it is necessary to fully consider the balance between the reactions and optimize the probe G Strand for HCV. We then designed five types of G-Strand 4 with different toeholds to test the displacement reaction between G-Strand and blocked guider. From the results in Figure S11, G Strand 4 for HCV shows the best signal-to-noise ratio.

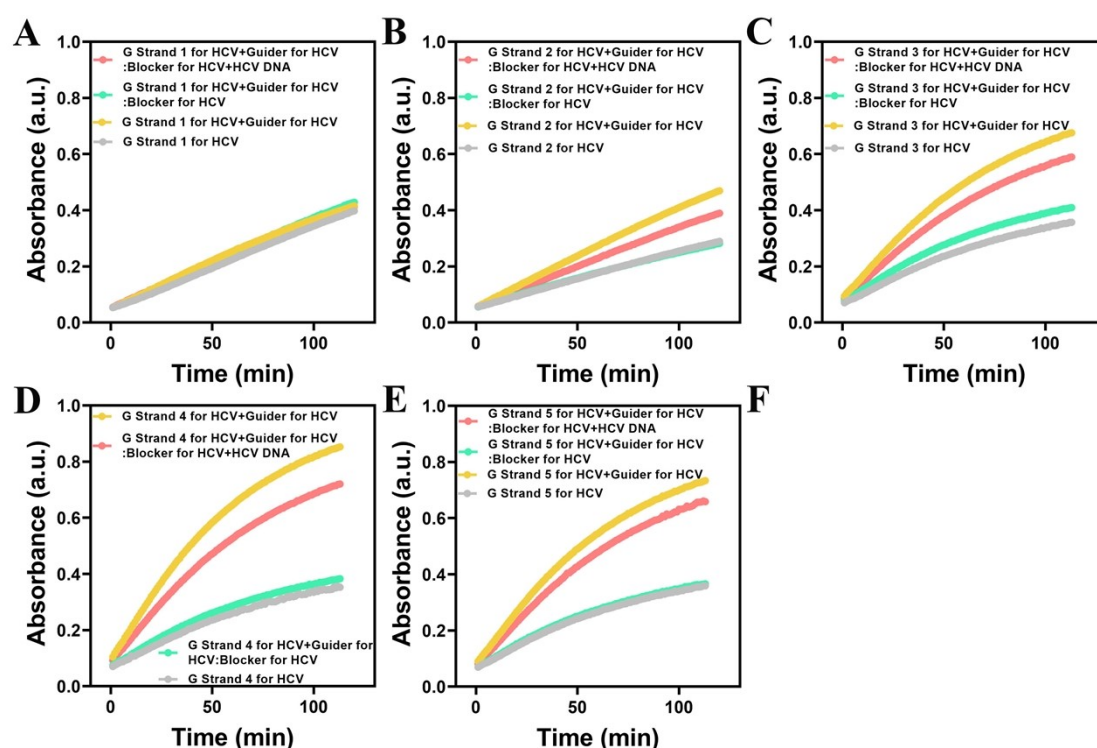


Figure S12. Sequence optimization of G Strand for HCV: (A) G Strand 1 for HCV; (B) G Strand 2 for HCV; (C) G Strand 3 for HCV; (D) G Strand 4 for HCV; and (E) G Strand 5 for HCV.

18. Specific response of the proposed sensing strategy to HCV DNA

The specificity was also examined by applying it to detection of five other sequences (Table S1) and the result in Figure S12 exhibited an acceptable specificity. The concentration of target (HCV DNA) was 50 nM, and the concentration of the interfering sequences was 500 nM (10-fold of the target).

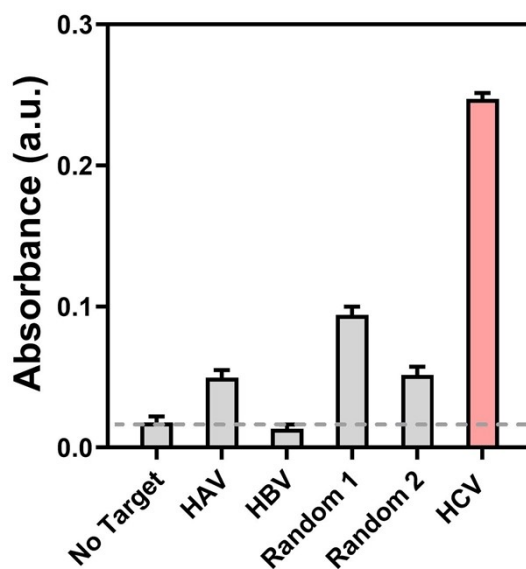


Figure S13. Specific response of the proposed sensing strategy to HCV DNA. Absorbance measurements were taken at 120 min (420 nm).

19. Guider with aptamer sequence in proposed strategy for PDGF-BB analysis

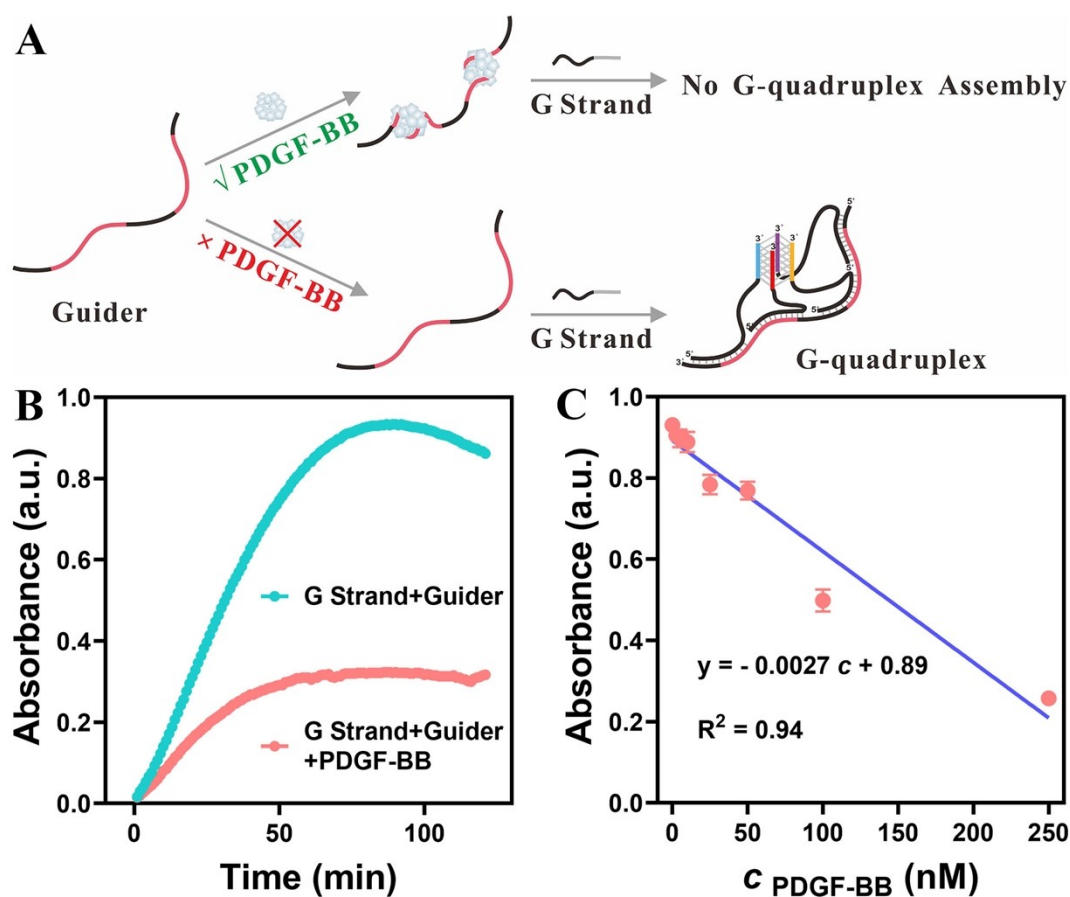


Figure S14. Application for PDGF-BB analysis. (A) The presence of PDGF-BB initiates the recognition event that deactivate the guider induced G-quadruplexes assembly. The determination of PDGF-BB can be achieved in turn-off manner; (B) various concentration of PDGF-BB activate the constructed strategy and give an absorbance change; and (C) response to different concentration of PDGF-BB: 0 nM, 2.5 nM, 5 nM, 10 nM, 25 nM, 50 nM, 100 nM, and 250 nM.

20. Specific response of the proposed sensing strategy to PDGF-BB

The specificity of the sensing platform for PDGF-BB was confirmed by the detection of several interfering proteins (Figure S14). The concentration of target (PDGF-BB) was 50 nM, and the interfering proteins included HSA, mucin, HEMO and TRF with the concentration of 500 nM (10-fold of the target), were detected respectively. The signal from the interfering proteins had no significant difference from that of the control group (No Target), and the addition of target (PDGF-BB) could significantly reduce the absorbance, which indicated a good specificity.

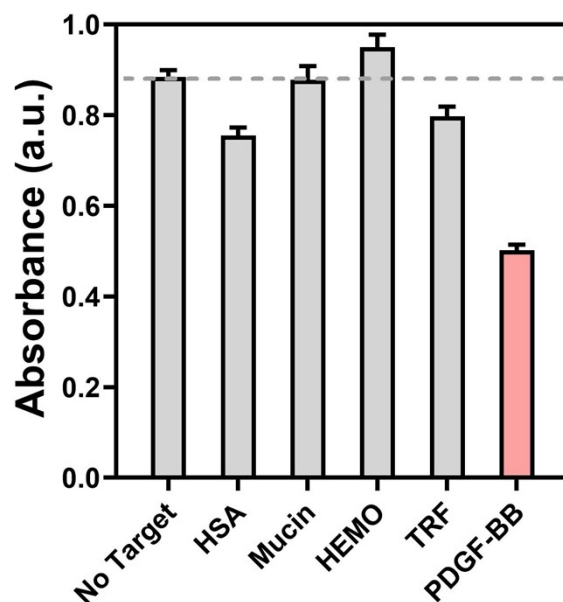


Figure S15. Specific response of the proposed sensing strategy to PDGF-BB. Absorbance measurements were taken at 120 min (420 nm).

21. PAGE Characterization of SA-guided Construction of G-quadruplex

To characterize SA-guided formation of intermolecular G-quadruplex structure, we performed the native PAGE (8%) analysis of SA, G strand with biotin and SA + G strand with biotin. The result of PAGE indicated that even there are a small part of G-quadruplex formed without SA, the existence of SA can effectively guide the assembly of tetramolecular G-quadruplex..

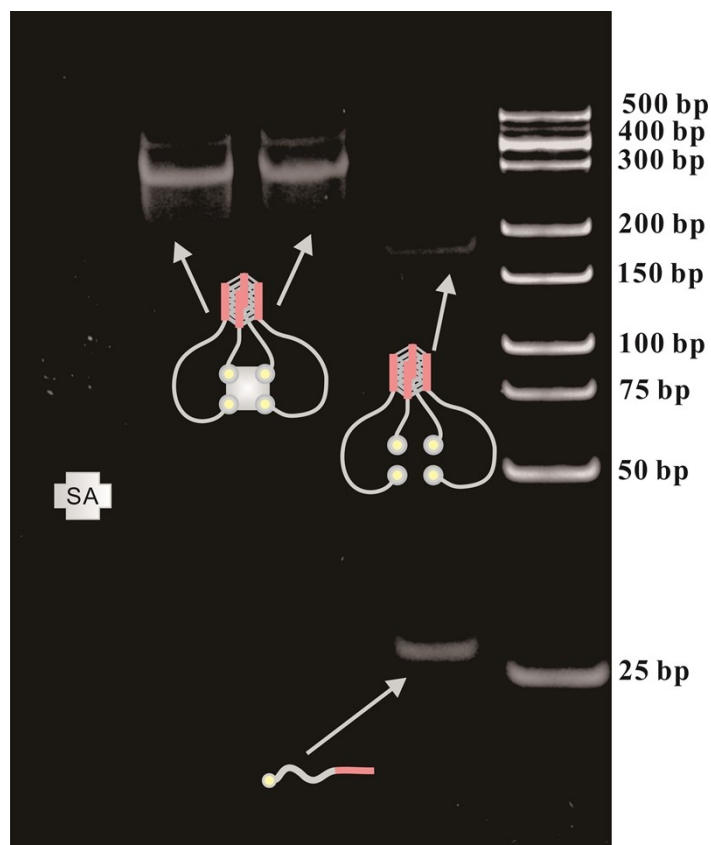


Figure S16. PAGE imaging of streptavidin (SA)-guided construction of G-quadruplex. To characterize SA-guided formation of intermolecular G-quadruplex structure, we performed the native PAGE (8%) analysis of streptavidin (SA) only, SA+ G strand with biotin and G strand with biotin only (from left to right)

22. AFM Characterization of SA-guided Construction of G-quadruplex

To characterize SA-guided formation of intermolecular G-quadruplex structure, AFM was applied to the analysis of free G strand with biotin (SA-G strand) and SA + G strand with biotin (SA-G strand). The result indicated that the existence of SA can effectively guide the assembly of tetramolecular G-quadruplex.

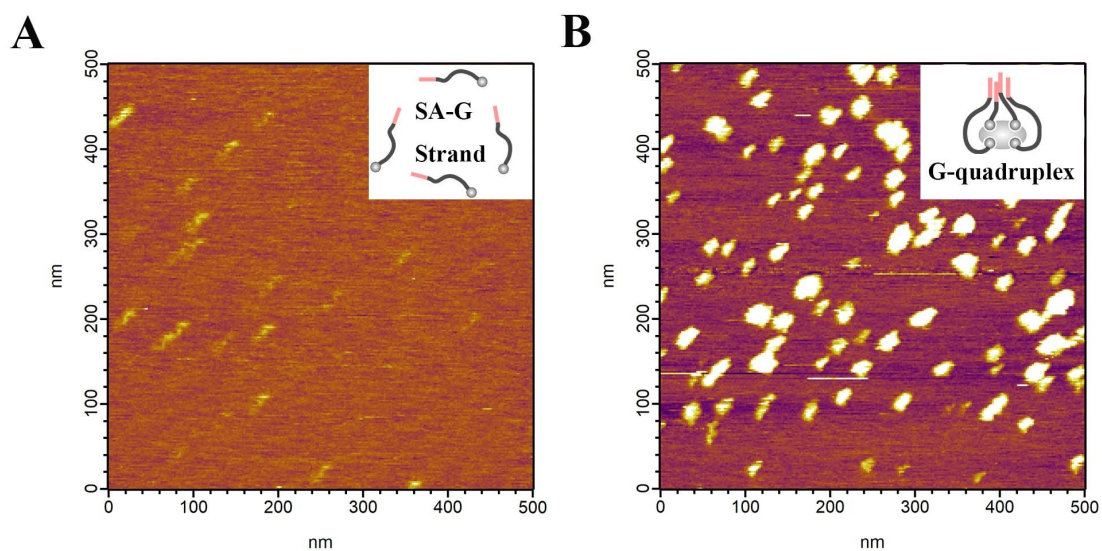


Figure S17. AFM imaging of SA-guided Construction of G-quadruplex: (A) SA-G Strand only, (B) SA + SA-G Strand.

23. Alpha-Fetoprotein (AFP) is employed directly as guider to induce G-quadruplexes assembly for analytical application

For the G-quadruplex Assembly, limited by the initial concentration of antibody, the concentration of AFP-G prepared is 100 nM, which is much lower than the other probe concentration (1 μ M). But AFP still acts as the guider, so that G can be assembled on it to increase the local concentration, thus enhancing the formation of G-quadruplex, which is manifested as the enhancement of absorption in Figure S17.

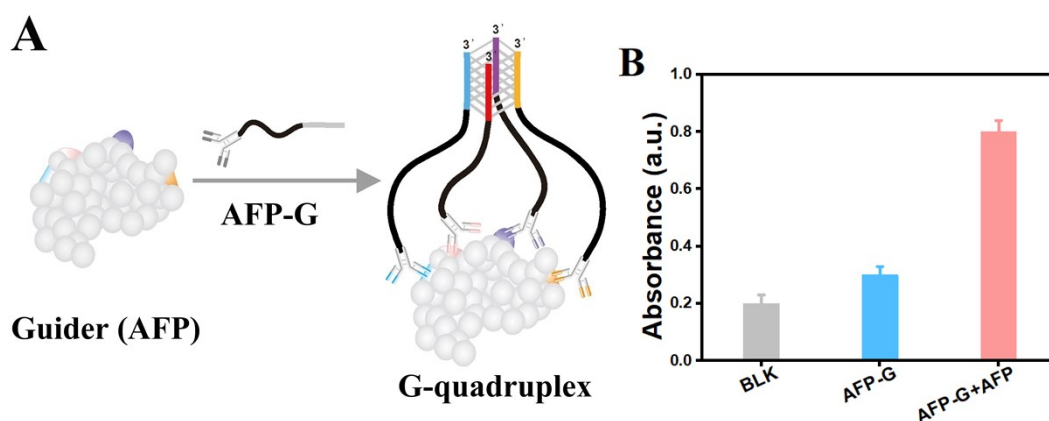


Figure S18. (A) Principle of AFP guided intermolecular G-quadruplexes self-assembly; and (B) presence of AFP activate the constructed system to increase the efficiency of G-quadruplexes formation and give an absorbance increasing. Absorbance measurements were taken at 120 min (420 nm).

Reference

1. N. Nagesh, D. Chatterji. *J. Biochem. Biophys. Methods* 1995, **30**, 1-8.
2. P. Schultze, N. V. Hud, F. W. Smith, J. Feigon. *Nucleic Acids Res.* 1999, **27**, 3018-3028.
3. A. Asati, C. Kaittanis, S. Santra, J. M. Perez. *Anal. Chem.* 2011, **83**, 2547–2553.
4. D. Li, B. W. Liu, P. J. J. Huang, Z. J. Zhang, J. W. Liu. *Chem. Commun.* 2018, **54**, 12519–12522.
5. J. Y. Zhang, S. H. Wu, X. M. Lu, P. Wu, J. W. Liu. *Nano Lett.* 2019, **19**, 3214-3220.
6. T. Muir, E. Morales, J. Root, I. Kumar, B. Garcia, C. Vellandi, D. Jenigian, T. Marsh, E. Henderson and J. Vesenska, *J. Vac. Sci. Technol. A*, 1998, **16**, 1172-1177.
7. K. Bose, C. J. Lech, B. Heddi and A. T. Phan, *Nat. Commun.*, 2018, **9**, 1959.
8. T. C. Marsh, J. Vesenska and E. Henderson, *Nucleic Acids Res.*, 1995, **23**, 696-700.
9. C. Kang, X. Zhang, R. Ratliff, R. Moyzis and A. Rich, *Nature*, 1992, **356**, 126-131.